

Maximum Flux Transition Paths of Conformational Change

Ruijun Zhao* and Robert D. Skeel†

Department of Computer Science, Purdue University

305 North University Street, West Lafayette, Indiana, 47907-2107

Juanfang Shen‡

Department of Mathematics, Purdue University

150 North University Street, West Lafayette, Indiana, 47907-2067

(Dated: May 13, 2022)

Abstract

Given two metastable states A and B of a biomolecular system, the problem is to calculate the likely paths of the transition from A to B . Such a calculation is more informative and more manageable if done for a reduced set of collective variables chosen so that paths cluster in collective variable space. The computational task becomes that of computing the “center” of such a cluster. A good way to define the center employs the concept of a committor, whose value at a point in collective variable space is the probability that a trajectory at that point will reach B before A . The committor “foliates” the transition region into a collection of isocommittors. The maximum flux transition path is defined as a path that crosses each isocommittor at a point which (locally) has the highest crossing rate of distinct reactive trajectories. (This path is different from that of the MaxFlux method of Huo and Straub.) To make the calculation tractable, three approximations are introduced. It is shown that a maximum flux transition path is at least qualitatively superior to a minimum free energy path, in particular when a minimum free energy path has cusps. These qualities aid in the construction of simple and robust algorithms. Such an algorithm and its performance is discussed.

PACS numbers: 81.15.Cc, 87.15.hp

Keywords: isocommittor; maximum flux transition path; minimum free energy path; reaction path; string method; transition path theory

I. SUMMARY

Considered here is the problem of computing transition paths of conformational change given two different metastable states of a biomolecule. One motivation for this is to facilitate the accurate calculation of free energy differences. Another motivation is to determine the existence and structure of transition states and intermediate metastable states. The latter are possible targets for inhibitors of enhanced specificity in cases where a family of proteins have active sites with very similar structure. A good example of this situation is Src tyrosine kinase, which has long been implicated in the development of cancer. For this system there are already computational results^{8,18,25}, the transition path from an active catalytic domain to an inactive catalytic domain.

Three major approaches to this problem are transition path sampling¹, transition path theory (TPT), and Markov state models²². For additional references, see, e.g., Ref.¹⁹. Here we pursue the approach of transition path theory^{6,15,16,23} because it is computationally feasible for larger proteins. The goal of this approach is to find one or several “representative” reaction paths connecting two given metastable states, each path representing a bundle or cluster of trajectories. In general, it may also be of interest to calculate (i) the reaction rate for each bundle, or, at least, the relative rate for different bundles, and (ii) the potential of mean force. Here we consider only the calculation of the path itself.

In a nutshell, this article embraces a certain aspect of TPT and carries it to a logical conclusion, obtaining a formula, an implementation, and a proof of concept. The claim is that we can do better than compute a minimum free energy path, namely, find a path which intersects each isocommittor at that point through which there is the highest number of crossings of *distinct* reactive trajectories. The task then is to explain what this means and provide supporting evidence.

A. Outline and discussion

There are two distinct steps in getting a solution: The first is to define the problem without considering what methods might be employed (other than taking into account what might be known about the intrinsic difficulty of the problem). Defining a problem apart from a method gives a more concise definition. Also, by not guessing about what is feasible

computationally, one may avoid unnecessary compromises. The second step is to construct a method and algorithm.

Given two metastable states A and B of a biomolecular system, the aim is to calculate the likely paths of the transition from A to B . Such a calculation is more informative and more manageable if done for a reduced set of *collective variables*, functions of the system configuration x ,

$$\zeta_1 = \xi_1(x), \zeta_2 = \xi_2(x), \dots, \zeta_\nu = \xi_\nu(x), \quad \text{abbreviated as } \zeta = \xi(x),$$

chosen so that paths cluster in collective variable space. The computational task becomes that of computing the “center” of such a cluster. A good way to define the center employs the concept of a committor, whose value at a point in collective variable space is the probability that a trajectory at that point will reach B before A . The committor “foliates” the transition region into a collection of committor isosurfaces known as isocommittors. The maximum flux transition path (MFTP) is defined as a path that crosses each isocommittor at a point which (locally) has the highest crossing rate of distinct reactive trajectories. The MFTP is not to be confused with MaxFlux method¹¹; it differs in several respects, e.g., the MFTP considers the flux of only those trajectories that are reactive (by using a result from TPT). A more detailed account of the problem definition is given in Section II.

To make the calculation tractable, three approximations are introduced. To make the committor a more accessible quantity, the set of paths is approximated by a Brownian dynamics model, resulting in a boundary value problem in ν -dimensional space. Then the number of space dimensions is reduced to one by assuming most of the transition paths are contained in a tube, resulting in a two-point boundary value problem with 2ν unknowns. A third approximation reduces this to ν unknowns, whose solution is a *maximum flux transition path*. This approximation involves a free energy gradient term and an explicitly temperature-dependent curvature term. Specifically, the maximum flux transition path $\zeta = Z(s)$, $0 \leq s \leq 1$, is defined by the condition that

$$-\beta \nabla F + \frac{(D(Z)^{-1} Z_s)_s}{Z_s^\top D(Z)^{-1} Z_s} \parallel D(Z)^{-1} Z_s,$$

holds for $\zeta = Z(s)$ where β is the inverse temperature, $F(\zeta)$ is the free energy profile, $D(\zeta)$ is a proto-diffusion tensor matrix depending on masses and ξ , and the subscript s denotes differentiation (d/ds). In the high temperature limit, the path becomes a straight line. In

the low temperature limit, the path becomes a minimum free energy path (MFEP). At zero temperature the path will have cusps at some intermediate local minima, which presents difficulties if free energy profiles or relative reaction rates are to be determined. Details are given in Section III.

The temperature-dependent curvature term not only provides a finite temperature correction to the MFEP, but it yields a nonsingular second order ordinary differential equation, amenable to standard techniques—except for the need to do computationally intensive sampling to evaluate terms in the differential equation. An existing set of algorithms for the MFEP^{4,15} applies equally well to the MFTP. The equation is discretized using upwinded differencing and solved using the simplified string method⁴. (A notable alternative is the nudged elastic band method, introduced in Ref.¹².) Algorithmic details are provided in Section IV.

Section V compares the MFTP to the MFEP on numerical examples. First an artificial problem in full configuration space is solved to demonstrate the effect of the curvature term of the MFTP. In particular, the necessity of using an adaptive mesh for the MFEP is demonstrated. Then alanine dipeptide in vacuum is solved using the phi, psi dihedrals as collective variables. For the transition path from $C_{7\text{ax}}$ to $C_{7\text{eq}}$ as in Ref.¹⁵, the computational cost for calculating the maximum flux transition path and the minimum free energy path is almost same. However, for a transition path from $C_{7\text{eq}}$ to $C'_{7\text{eq}}$ through $C_{7\text{ax}}$ shown in Ref.²⁰, the minimum free energy path has a cusp at $C_{7\text{ax}}$ and the computational cost for finding such a cusp is expensive. On the other hand, the maximum flux transition path smooths out the cusp and the computational cost is dramatically reduced.

An open source implementation of the MFTP method is available²⁶ as a relatively simple set of Python modules with examples using pure Python, CHARMM, and NAMD.

II. WHAT IS THE PROBLEM?

We begin by defining an ensemble of transition paths from A to B : For simplicity, assume the molecular system obeys Newtonian dynamics with potential energy function $U(x)$ and a diagonal matrix M of atomic masses. Positions x and momenta p satisfy $x = X(t)$, $p = P(t)$ where $(d/dt)X(t) = M^{-1}P(t)$ and $(d/dt)P(t) = -\nabla U(X(t))$. Initial values are drawn from a Boltzmann-Gibbs distribution $\rho(x, p)$: positions x from probability density $const e^{-\beta U(x)}$

and momenta p from a Maxwell distribution. Imagine an extremely long trajectory. The trajectory enters and leaves A and B many times yielding a huge set of reactive paths from A to B . (A reactive path is a piece of the trajectory outside of A and B that comes from A and goes to B .)

Generating an ensemble of trajectories is extremely demanding computationally. And, even if this were possible, what would the user do with all the data? By answering such a question, we might well avoid the task of computing trajectories. It is likely that one would cluster the trajectories to produce a concise description. Therefore, one might instead directly determine such a concise description. Specifically, if the paths cluster into one or several distinct isolated bundles/tubes/channels/pathways, one might compute a “representative path” for each cluster. This idea is developed in the paragraphs that follow.

However, transition paths might not cluster adequately—in full configuration space. Assume, though, there is a smaller set of collective variables, $\zeta = \xi(x)$, such that in ζ -space, paths cluster into one or several distinct isolated channels connecting two separated subsets A_ξ and B_ξ of collective variable space. Otherwise, there is little of interest to compute. A typical example of collective variables is phi/psi angles along a peptide backbone. Once the collective variables are specified, the problem is to calculate a path in collective variable space, $\zeta = Z(s)$, $0 \leq s \leq 1$, connecting A_ξ to B_ξ where the transition paths are concentrated. Along with a parameterization of the path in collective variables coordinates, would be a realization of it in cartesian coordinates, so once the path is generated, structures can be studied as well. A drawback of this approach is the need to identify an appropriate set of collective variables.

We want a minimal set of collective variables subject to two conditions: First, the coordinates ζ must suffice to describe states A_ξ , B_ξ in ζ -space corresponding to A , B . Second, coordinates ζ must also be rich enough to “express the mechanism of conformational change” along the transition path. To make the second condition more precise, we introduce the notion of “quasi-committor.”

To measure the progress of a transition, there is a natural reaction coordinate, known as the *committor*. This concept of a commitment probability was introduced by Onsager¹⁷, and the abbreviated term “committor” was introduced in Ref.² (p. 9236), which they defined as follows: For each point x in configuration space, consider a trajectory starting with $X(0) = x$ and velocities drawn at random from a Maxwell distribution, and define the committor $q(x)$

to be the probability of reaching B before A . Since it is the coordinates of the collective variables that are of interest, it is natural also to define a *quasi-committor*: For each point ζ , consider a trajectory starting with random initial values *conditioned on* $\xi(x) = \zeta$ and define the quasi-committor $\hat{q}(\zeta)$ to be the probability of reaching B_ζ before A_ζ :

$$\hat{q}(\zeta) = \Pr(\xi(X(t)) \text{ reaches } B_\zeta \text{ before } A_\zeta \mid \xi(X(0)) = \zeta).$$

We could say that the variables $\zeta = \xi(x)$ are rich enough to express the mechanism of conformational change if the quasi-committor $\hat{q}(\zeta)$ has no local minima or maxima outside of A_ζ and B_ζ (except for regions of negligible probability). Otherwise, there is some unexpressed degree of freedom important to the transition, as illustrated in Fig. 1.

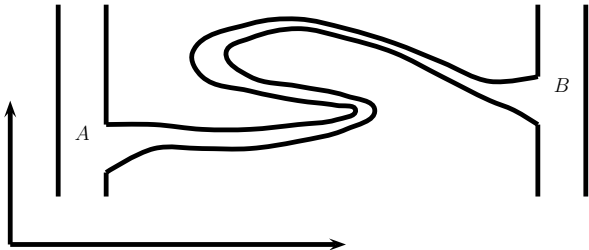


FIG. 1: A schematic illustration of a poor choice of collective variables. The horizontal axis is collective variables, and the vertical axis is unrepresented degrees of freedom. The collective variables fail to indicate the progress of the reaction.

The quality of the collective variables can be checked in principle by calculating quasi-committor values $\hat{q}(\zeta)$ at points along the path from dynamics trajectories.

There are several ways to define the “center” of a cluster of paths in ζ -space, including the following:

1. a most probable path, e.g., swarm-of-trajectories string method¹⁹,
2. a *maximum flux path*, which is our choice, and
3. a center-of-flux path, e.g., finite temperature string method²⁰.

The MFEP is a limiting case of both definitions 1 and 2.

The most probable path tends to be a path of minimum energy, and it is not clear that this is a “representative” path. For Hamiltonian dynamics, it would seem that the probability

that we attach to a path would be proportional to $\exp(-\beta E)$ where E is the energy. Hence, the most probable path is the one with just enough energy to surmount the potential energy barriers. For stochastic dynamics, the explanation of how to assign probability to paths is quite complicated—if paths of different durations are being compared. An explanation for Brownian dynamics requires Freidlin-Wentzell theory and the assumption of vanishingly small noise¹⁵ (Appendix A).

The second and third definitions of a representative path are in terms of isosurfaces of the quasi-committor. On each such isosurface, consider the distribution $j(\zeta)$ of distinct crossing points from reactive trajectories in collective variable space. Choose the “center” of this distribution to be the point where the path crosses the quasi-committor isosurface. This approach is not well represented in literature. An exception is Ref.¹⁶ (Sec. III.C), which emphasizes the density of crossings of a surface by distinct reactive trajectories, instead of all crossings by reactive trajectories.

One way to define a distribution of distinct reactive trajectories makes use of the concept of last hitting points. Ref.⁶ uses this to define a vector field $J(\zeta)$, whose significance is best explained in terms of an integral over an arbitrary subset Σ' of a surface Σ that separates collective variable space into two parts, one containing A_ξ and the other containing B_ξ : the probability current $J(\zeta)$ is such that the integral

$$\int_{\Sigma'} J(\zeta) \cdot \hat{n}(\zeta) dS_\zeta$$

gives the rate of last crossing of Σ' by reactive trajectories from one side to the other side, where $\hat{n}(\zeta)$ is a normal vector pointing to the other side of Σ . If $\Sigma' = \Sigma$, the integral gives the reaction rate k_{AB} . The density of last hitting points is then given by the normal flux $j(\zeta) = J(\zeta) \cdot \hat{n}(\zeta)$ on each quasi-committor isosurface Σ .

One can define the center of a bundle of transition paths to be that point on each quasi-committor isosurface that maximizes the density $j(\zeta)$ of last hitting points. In other words, seek the path $\zeta = Z(s)$, $0 \leq s \leq 1$, each of whose points $Z(s)$ is a local maximum of the density of distinct trajectories $j(\zeta)$ on the quasi-committor isosurface Σ passing through $Z(s)$.

Another choice, associated with the *finite-temperature string method*, is to construct the path from the “mean” value ζ' on each quasi-committor isosurface Σ : the point ζ' that minimizes $\int_\Sigma |\zeta' - \zeta|^2 j(\zeta) d\zeta$. The equations defining such a center-of-flux path are intrinsically

more expensive computationally to solve than those for the maximum flux path, because they require averaging on isosurfaces rather than merely determining a (local) maximum. Also, this notion of a path is more complicated.

III. A METHOD

As stated previously, computing $\hat{q}(\zeta)$ is not feasible. Consequently, we derive a method, which employs three uncontrolled approximations—a controlled approximation being one that can be made arbitrarily accurate with sufficient computational effort.

A. Brownian dynamics approximation of collective variable paths

This material is adapted from Ref.¹⁵ (Sec. III, A and B).

The quasi-committor is related to a full phase-space committor in Ref.²³ (Sec. 6.2) q^* defined as follows:

$$q^*(x, p) = \Pr(X(t) \text{ reaches } B \text{ before } A \mid X(0) = x, P(0) = p).$$

Note that $q^*(x, p) = 0$ or 1 , because the dynamical equation is deterministic. The p.d.f. for $\xi(x)$ is

$$\rho_\xi(\zeta) = \langle \delta(\xi(x) - \zeta) \rangle = \int \int \delta(\xi(x) - \zeta) \rho(x, p) dx dp$$

where $\delta(\zeta) = \delta(\zeta_1)\delta(\zeta_2)\cdots\delta(\zeta_\nu)$. Let $\langle \cdot \rangle_\zeta$ be the expectation for the conditional density $\rho(x, p | \xi(x) = \zeta)$:

$$\langle O(x) \rangle_\zeta = \frac{\langle \delta(\xi(x) - \zeta) O(x) \rangle}{\langle \delta(\xi(x) - \zeta) \rangle}.$$

Hence, the quasi-committor $\hat{q}(\zeta) = \langle q^*(x, p) \rangle_\zeta$.

It is not difficult to show that $\hat{q}(\xi(x))$ approximates $q^*(x, p)$ in the sense that it minimizes $\langle |q(\xi(x)) - q^*(x, p)|^2 \rangle$ over all $q(\zeta)$. However, this is not useful for determining $\hat{q}(\zeta)$ because $q^*(x, p)$ is too costly to compute. On the other hand, it is possible to find a best approximation to $q^*(x, p)$ in another sense. Because q^* is constant on a trajectory, we have

$$0 = \frac{d}{dt} q^*(X(t), P(t)) = (Lq^*)(X(t), P(t)) \quad \text{where } L = (M^{-1}p) \cdot \nabla_x - U_x \cdot \nabla_p.$$

Consequently, q^* satisfies the stationary Liouville equation

$$Lq^* = 0, \quad q^* = 0 \text{ on } A, \quad q^* = 1 \text{ on } B.$$

Since we do know $Lq^* = 0$, we seek instead an approximation q that minimizes $I(q) = \langle |L(q(\xi(x)) - q^*(x, p))|^2 \rangle$, a standard tactic in numerical analysis. This simplifies to

$$I(q) = \frac{1}{\beta} \langle |M^{-1/2} \nabla_x q(\xi(x))|^2 \rangle,$$

which is to be as small as possible. A low value for $I(\hat{q})$ is attained by having $\hat{q}(\zeta)$ increase monotonically from the value 0 on A_ξ to the value 1 on B_ξ , which is consistent with the prescription given earlier that $\xi(x)$ be chosen so that the quasi-committor has no local minima or maxima outside of A_ξ and B_ξ .

The functional $I(q)$ can be expressed in terms of collective variables ζ . Define the free energy $F(\zeta)$ for coordinates $\zeta = \xi(x)$ by

$$\text{const}_\xi e^{-\beta F(\zeta)} = \rho_\xi(\zeta) = \langle \delta(\xi(x) - \zeta) \rangle.$$

Also define a proto-diffusion tensor D by

$$D(\zeta) = \frac{1}{2} \beta^{-1} \langle \xi_x(x) M^{-1} \xi_x(x)^\top \rangle_\zeta.$$

(The tensor $D(\zeta)$ fails to be a diffusion tensor because it is missing a time scale factor.) The functional can then be written¹⁵

$$I(q) = \text{const}_\xi \int e^{-\beta F(\zeta)} \nabla q(\zeta)^\top D(\zeta) \nabla q(\zeta) d\zeta \quad (1)$$

where the integral is over the transition region outside of A_ξ and B_ξ subject to $q(\zeta) = 0$ on the boundary of A_ξ and $q(\zeta) = 1$ on the boundary of B_ξ .

The corresponding Euler-Lagrange equation for $q(\zeta)$ is the Smoluchowski (backward Kolmogorov) equation:

$$-\nabla \cdot e^{-\beta F(\zeta)} D(\zeta) \nabla q(\zeta) = 0, \quad (2)$$

subject to $q(\zeta) = 0$ on the boundary of A_ζ and $q(\zeta) = 1$ on the boundary of B_ζ .

The function q that satisfies the Smoluchowski equation subject to the given boundary conditions can be shown to be the exact committor function for paths $\zeta = \zeta(\tau)$ in collective variable space generated by the Brownian dynamics

$$\frac{d}{d\tau} \zeta = -\beta D(\zeta) \nabla F(\zeta) + (\nabla \cdot D(\zeta))^\top + \sqrt{2} D_{1/2}(\zeta) \eta(\tau) \quad (3)$$

where $D_{1/2} D_{1/2}^\top = D$ and $\eta(\tau)$ is a collection of standard white noise processes. The fact that τ is an artificial time does not affect the committor. In principle, the assumption

$q^*(\xi(x), p) \approx \hat{q}(\zeta)$ can be checked a posteriori by comparing committor values of the Brownian dynamics to the quasi-committor values of actual dynamics.

Reference¹⁵ (Sec. III.C) appears to suggest that the Smoluchowski equation uniquely specifies dynamics except for scaling of time: If the Smoluchowski equation (2) is satisfied by committors $q(\zeta)$ for arbitrary sets A'_ζ and B'_ζ in collective variable space, then the paths whose committor functions satisfy Equation (2) must be those of the Brownian dynamics. Hence, paths $\zeta = \zeta(\tau)$ in collective variable space can be generated with the proper probabilities from the system of stochastic differential equations.

B. Last hitting-point distribution

The proof of Proposition 5 in Ref.⁶ (p. 518) analyzes the flux of reactive trajectories across an arbitrary surface Σ that separates collective variable space into two parts, one containing A_ξ and the other containing B_ξ . The proof actually looks not at all crossings but only those occurring within a vanishingly small time interval before the last crossing. See Eq. (50) of Ref.⁶. Therefore, it considers the net flux only in this limiting sense. As the length of the time interval $\tau \rightarrow 0$, the positions of these crossings all converge to the position of the last crossing. So, indeed, one gets the flux of the last hitting point from Proposition 5 of Ref.⁶. The result given in Ref.⁶ (Eq. (39)), as well as in Ref.¹⁶ (Eq. (6), Eq. (A12)), and Ref.²³ (Eq. (62)), is that the last hitting-point flux for reactive trajectories is

$$J(\zeta) = \rho_\xi(\zeta) D(\zeta) \nabla q(\zeta),$$

meaning that the integral

$$\int_{\Sigma} J(\zeta) \cdot \hat{n}(\zeta) dS_{\zeta},$$

where $\hat{n}(\zeta)$ points to the side containing B_ξ , gives the rate of the *last* crossing of Σ by reactive trajectories. (Proposition 4 of Ref.⁶ does not apply to the infinitely damped case of Langevin dynamics.)

If Σ is an isocommittor, it has a normal given by $\hat{n}(\zeta) = \nabla q(\zeta) / |\nabla q(\zeta)|$, so the distribution of last hitting points on an isocommittor is therefore proportional to

$$j(\zeta) = \rho_\xi(\zeta) \nabla q(\zeta)^T D(\zeta) \nabla q(\zeta) / |\nabla q(\zeta)|.$$

There is an example in Metzner, Schuette, and Vanden-Eijnden (2006) section III.C, where it is suggested to use $\hat{n} \cdot J$. This formula is confirmed in the special case $D = I$ by the

first hitting point distribution given in Ref.²⁴ (Appendix B). Last and first are the same for reversible dynamics like Brownian dynamics.

C. Defining the path

For computation it is convenient to label the isocommittors with the path parameter s . In particular, denote by $\Sigma(s)$, $0 \leq s \leq 1$, the isocommittor passing through $\zeta = Z(s)$. For a given value of s , let $\bar{q}(s) = q(Z(s))$ be the corresponding committor value. Hence

$$\sigma(\zeta) \stackrel{\text{def}}{=} \bar{q}^{-1}(q(\zeta))$$

gives the label s of the isocommittor passing through an arbitrary point ζ . In this way the committor $q(\zeta)$ is decomposed into two independent parts: one part $\sigma(\zeta)$ specifies isocommittors and the other part $\bar{q}(s)$ calibrates the isocommittors. On an isocommittor $\Sigma(s)$, the gradient $\nabla q(\zeta) = (d\bar{q}(s)/ds)\nabla\sigma(\zeta)$, so the normal flux is

$$j(\zeta) = (d\bar{q}(s)/ds)\rho_\xi(\zeta)\nabla\sigma(\zeta)^\top D(\zeta)\nabla\sigma(\zeta)/|\nabla\sigma(\zeta)|.$$

Note that \bar{q} contributes only a scale factor to $j(\zeta)$, so the center of intensity on $\Sigma(s)$ does not depend on \bar{q} .

Each point $Z(s)$ on the desired path maximizes the last-hitting flux $j(\zeta)$ on the isocommittor $q(\zeta) = q(Z(s))$. Hence, $\nabla j(Z(s)) \parallel \nabla q(Z(s))$. To keep the derivation independent of the calibration $\bar{q}(s)$, introduce a vector $n(s)$, not necessarily normalized, such that $n(s) \parallel \nabla q(Z(s))$. Hence,

$$\nabla j(Z(s)) \parallel n(s).$$

D. The localized tube assumption

Assume there exists a tube connecting A_ζ to B_ζ such that (i) on each isocommittor, regions of high $j(\zeta)$ are concentrated in the tube, (ii) each isocommittor is nearly planar in the tube, and (iii) $D(\zeta)$ is nearly constant on each isocommittor within the tube. This scenario is illustrated in Fig. 2 below.

Exploit the localized tube assumption by approximating the isocommittor through $Z(s)$ as a plane $\Pi(s)$ with normal $n(s)$. Hence, the isocommittor surface $\Sigma(s) : \sigma(\zeta) = s$ has the

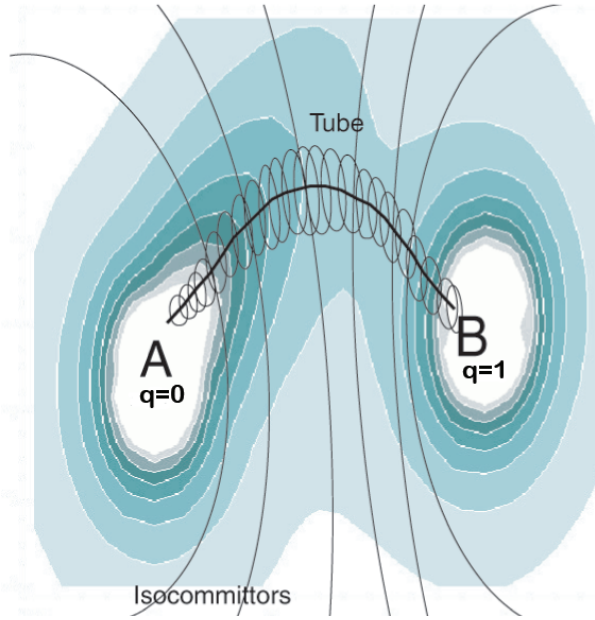


FIG. 2: Shading indicates contours of free energy, thin curves denote isocommittors, ellipses enclose concentrations of crossing points from reactive trajectories, and the thick curve is the center.

simple description of a hyperplane,

$$\Pi(s) : \quad n(s) \cdot (\zeta - Z(s)) = 0.$$

Also, approximate $D(\zeta)$ by $\bar{D}(\sigma(\zeta))$ where $\bar{D}(s) \stackrel{\text{def}}{=} D(Z(s))$. These approximations (see Ref.²³ (Sec. 6.6.1)) are sufficient to define a practical method (see Ref.⁵ (Sec. 12)). The unknown direction vector $n(s)$ is to be chosen to minimize the integral $I(q)$ of Eq. (1) restricted to some tube. For simplicity the boundary points $Z(0)$ and $Z(1)$ can be moved to points in A_ζ and B_ζ that locally minimize $F(\zeta)$. In this way the problem of solving for a committor of many variables is reduced to that of a one-dimensional calculation along the length of the tube.

It remains to derive the condition that determines $Z(s)$. This is done in Appendix A, where it is shown that the condition is

$$-\beta \nabla F(Z) + \frac{n_s}{n^\top Z_s} \parallel n.$$

E. The maximum flux transition path

Although the localized tube assumption is sufficient for defining a practical method, the method would not be simple, so we make an additional simplifying assumption: Assume that on each isocommittor, the probability is strongly peaked around the path (see Ref.²³ (Sec. 6.6)). Because a narrow tube contains most of the probability, the flux $J(\zeta)$ points in the direction of the tube and the path, which motivates the approximation $J(Z(s)) \parallel (d/ds)Z(s)$ or $D(Z(s))\nabla q(Z(s)) \parallel (d/ds)Z(s)$, whence

$$n(s) \parallel D(Z(s))^{-1} \frac{d}{ds} Z(s).$$

The result is a *maximum flux transition path*

$$-\beta \nabla F(Z) + \frac{(D(Z)^{-1} Z_s)_s}{Z_s^\top D(Z)^{-1} Z_s} \parallel D(Z)^{-1} Z_s. \quad (4)$$

Geometrically this condition means that in addition to decreasing the free energy orthogonal to the path, we also move in the direction of the center of the radius of curvature, thus reducing the curvature and inhibiting cusps.

Write condition (4) as $-\beta(Z_s^\top D^{-1} Z_s) D \nabla F + D(D^{-1} Z_s)_s = \lambda Z_s$ where λ is a scalar and premultiply by Z_s^\top to obtain $\lambda = (-\beta(Z_s^\top D^{-1} Z_s) Z_s^\top D \nabla F + Z_s^\top D(D^{-1} Z_s)_s) / (Z_s^\top Z_s)$. After eliminating λ , the equation becomes

$$(I - \Pi) D(D^{-1} Z_s)_s = (I - \Pi) \beta (Z_s^\top D^{-1} Z_s) D \nabla F \quad (5)$$

where the projector

$$\Pi = Z_s Z_s^\top / (Z_s^\top Z_s).$$

Note that, if D is constant, the limit $\beta \rightarrow 0$ for Eq. (5) gives a geodesic $Z_{ss} = 0$, which is the desired result.

In 2D with $D = I$, the Euclidean length of $(I - \Pi) D(D^{-1} Z_s)_s / (Z_s^\top D^{-1} Z_s)$ is exactly equal to the curvature, which is defined to be the reciprocal of the radius of curvature. To see this, note that this is true if we parameterize with (actual) arc length and note also that the curvature term is independent of parameterization (which can be checked analytically).

If we normalize the parameterization using $(Z_s^\top Z_s)_s = 0$, this implies $Z_s^\top Z_{ss} = 0$ and $\Pi Z_{ss} = 0$. Adding this last equation to Eq. (5) gives a *nonsingular* second order ordinary differential equation for $Z(s)$:

$$Z_{ss} = (I - \Pi) (\beta (Z_s^\top D^{-1} Z_s) D \nabla F + D_s D^{-1} Z_s).$$

One way to analyze a transition is to calculate the free energy $F(Z(s))$ along the path by integrating values obtained from constructing the path,

$$F(Z(s)) - F(Z(0)) = \int_0^s \nabla F(Z(s'))^\top \frac{d}{ds'} Z(s') ds',$$

and use the value of s that maximizes $F(Z(s))$ for the transition state. This is a quick but not so accurate way to determine the transition state¹⁵ (Sec. III.D), since $F(Z(s))$ is not a PMF for the transition.

F. The minimum free energy path

The simplifying assumption that is used to derive the MFTP is based on the low temperature limit $\beta \rightarrow \infty$; see Ref.²³ (Sec. 6.6) and Ref.¹⁵ (App. A). A more systematic derivation would therefore neglect the curvature term. The result would be a *minimum free energy path*

$$Z_s \parallel -\beta D(Z) \nabla F(Z).$$

Each point $\zeta = Z(s)$ on the minimum free energy path is a local minimum of $F(\zeta)$ in the hyper-plane orthogonal to $D(Z(s))^{-1}(d/ds)Z(s)$.

One difference from an MFTP is that an MFEP can have a cusp at an intermediate local minimum. If the path passes sufficiently close to a local minimum $\zeta = \zeta_0$ of $F(\zeta)$, then for a short section of the path, $\zeta = Z(s)$, $a \leq s \leq b$, a quadratic approximation to $F(\zeta)$ is accurate. Assume $D = \text{constant}$ and $F(\zeta) = \frac{1}{2}(\zeta - \zeta_0)^\top A(\zeta - \zeta_0) + \text{constant}$, where A is symmetric positive definite. The MFEP is then defined by $Z_s \parallel -\beta D A(Z - \zeta_0)$. Perform a change of variables, $Y = \beta^{-1/2} Q^\top D_{1/2}^{-1}(Z - \zeta_0)$ where $Q \Lambda Q^\top$ is a diagonalization of $D_{1/2}^\top A D_{1/2}$. The MFEP for $Y(s)$ is hence given by $Y_s \parallel -\Lambda Y$. For simplicity, suppose that $Y = [x, y]^\top$, that $x(a) < 0 < x(b)$, and that $\Lambda = \text{diag}(\lambda, \mu)$ with $\lambda > \mu$. The path is hence defined by $y_s/(\mu y) = x_s/(\lambda x)$, which can be integrated to yield the path

$$y = \begin{cases} (x/x(a))^{\mu/\lambda} y(a), & x(a) \leq x \leq 0, \\ (x/x(b))^{\mu/\lambda} y(b), & 0 \leq x \leq x(b), \end{cases}$$

which has a cusp at $x = 0$.

The presence of cusps undermines the localized tube assumption. In particular, the assumption of isocommittors being approximately planar breaks down at a cusp. This poses

a difficulty when computing transition rates, which depends on existence of isocommittors. Additionally, cusps complicate the numerical approximation of paths.

IV. AN ALGORITHM

An algorithm for calculating a transition path employs a progression of four controlled approximations: a discretization of the path $\zeta = Z(s)$ and the conditions that define it; iteration error in the solution of nonlinear discrete equations; blurring, due to use of restraints for constrained sampling; and statistical error due to finite sampling.

A. Discretization

The path $Z(s)$, $0 \leq s \leq 1$, is approximated as a piecewise polynomial with break points $0 = s_0 < s_1 < \dots < s_J = 1$. Here we choose a uniform mesh $s = 0, \Delta s, \dots, 1$ and obtain the path by piecewise linear interpolation. Thus the problem is reduced to determining *unknown* nodal values $Z_j \approx Z(s_j)$, $j = 0, 1, \dots, J$, each representing a replica of the system in a different configuration.

It is convenient for computation to use for the path parameter s the arc length along the path divided by the total length of the path. In such a case, $|(d/ds)Z(s)|$ is constant. The arc length normalization becomes

$$|Z_{j+1} - Z_j|\Delta s = |Z_j - Z_{j-1}|\Delta s, \quad j = 1, 2, \dots, J - 1.$$

Condition (4) is discretized by first multiplying by $Z_s^T D^{-1} Z_s$ to isolate the second derivative term, then integrating with each of the piecewise linear basis functions as a test function, doing an integration by parts on the second derivative term, and applying a composite trapezoid quadrature rule. The result is

$$-\beta(Z_s^T D^{-1} Z_s)_j (\nabla F)_j + ((D^{-1} Z_s)_s)_j \parallel D_j^{-1} (Z_s)_j$$

where

$$\begin{aligned} (Z_s^T D^{-1} Z_s)_j &= \frac{1}{2} \Delta s^{-2} (\Delta_- Z_j^T D_j^{-1} \Delta_- Z_j + \Delta_+ Z_j^T D_j^{-1} \Delta_+ Z_j), \\ ((D^{-1} Z_s)_s)_j &= \Delta s^{-2} ((D^{-1})_j^+ \Delta_+ Z_j - (D^{-1})_j^- \Delta_- Z_j) \end{aligned} \quad (6)$$

with

$$\Delta_{\pm} Z_j = \mp (Z_j - Z_{j\pm 1}) \quad \text{and} \quad (D^{-1})_j^{\pm} = \frac{1}{2} (D_j^{-1} + D_{j\pm 1}^{-1}).$$

Hence,

$$(Z_s)_j \parallel g_j, \quad \text{where } g_j = D_j \left(-\beta(\nabla F)_j + \frac{((D^{-1}Z_s)_s)_j}{(Z_s^\top D^{-1}Z_s)_j} \right).$$

We choose upwinded differencing for $(Z_s)_j$ based on the direction of the modified mean force g_j :

$$(Z_s)_j = \begin{cases} (Z_j - Z_{j-1})\Delta s & \text{if } g_j^\top(Z_j - Z_{j-1}) > 0, \\ (Z_{j+1} - Z_j)\Delta s & \text{if } g_j^\top(Z_j - Z_{j+1}) > 0. \end{cases} \quad (7)$$

In the unlikely event that both conditions are satisfied, the choice is dictated by the arc length normalization step of the simplified string method to be discussed next.

MFEP would have cusps at some intermediate local minima, which requires adaptive discretization methods.

B. Solution of nonlinear discrete equations

A second component of an algorithm is an iterative method for achieving rapid local convergence given a plausible initial guess.

For large systems, targeted molecular dynamics²¹ has been used to get an initial path^{8,10}. Another potentially promising but quite different approach is rigidity analysis¹³.

Because of its simplicity and demonstrated effectiveness, we adopt the simplified string method using the descent direction given by condition (4). To determine a path, begin with an initial guess and generate successive improvements by alternating between moving the points of the curve Z_j in the direction g_j given by condition (4) and reparameterizing:

$$Z_j^* = Z_j + \tau^2 g_j, \quad Z_j^{\text{new}} = Z_j^* + \text{normalization adjustment}. \quad (8)$$

(The extra factor τ provides the time scale factor missing from D .) The normalization adjustment is to choose the $\{Z_j\}$ to be equidistant along the resulting curve:

$$\begin{aligned} s_0^* &= 0, s_j^* = s_{j-1}^* + |Z_j^* - Z_{j-1}^*|, \\ Z^*(s) &= \text{piecewise linear interpolation of } \{(s_j^*/s_j^*, Z_j^*)\}, \quad 0 \leq s \leq 1, \\ Z_j^{\text{new}} &= Z^*(j/J). \end{aligned}$$

Also the endpoints Z_0 and Z_J are moved towards local minima if they are not already there. It can be shown that if the simplified string method converges, it converges to a discretization of the differential equations that becomes upwinded differencing in the limit $\tau \rightarrow 0$.

C. Conditional averages

Evaluation of $\nabla F(Z(s))$ and $D(Z(s))$ at break points involves sampling on hyper-surfaces $\{x : \xi(x) = Z(s)\}$ of configuration space.

For calculating such conditional expectations, the Dirac delta function $\delta(s)$ can be approximated by the p.d.f. of a Gaussian $\delta_\varepsilon(s) = (2\pi\varepsilon^2)^{-1/2} \exp(-s^2/(2\varepsilon^2))$. Note

$$\delta_\varepsilon(\xi(x) - \zeta) e^{-\beta U(x)} = (2\pi\varepsilon^2)^{-\nu/2} e^{-\beta U(x; \zeta)}$$

where

$$U(x; \zeta) = U(x) + \sum_{i=1}^{\nu} u_i(x, \zeta_i), \quad \text{and } u_i(x, \zeta_i) = \frac{1}{2\beta\varepsilon^2} (\xi_i(x) - \zeta_i)^2. \quad (9)$$

The effect is that of using restraining potentials instead of constraints. These restraints should be as strong as possible without restricting the step size used in the sampling. Then,

$$D(\zeta) = \frac{1}{2} \beta^{-1} \langle \xi_x M^{-1} \xi_x^\top \rangle_\zeta, \quad \text{where } \langle O(x) \rangle_\zeta = \frac{\langle O(x) \delta_\varepsilon(\xi(x) - \zeta) \rangle}{\langle \delta_\varepsilon(\xi(x) - \zeta) \rangle}.$$

Note that $\langle O(x) \rangle_\zeta$ is nothing but an average using $U(x; \zeta)$. From $\text{const}_\xi \exp(-\beta U(x; \zeta)) = \langle \delta_\varepsilon(\xi(x) - \zeta) \rangle$, we have

$$\nabla F(\zeta) = -\frac{1}{\beta\varepsilon^2} \langle \xi(x) - \zeta \rangle_\zeta.$$

Analytical values for ξ_x can be obtained using CHARMM³ by evaluating forces with restraints $\xi_i(x) \approx \zeta_i - c$ selectively turned on, where c is a number so that $\xi_i(x) - \zeta_i \neq c$ for all x ⁹. In particular,

$$\frac{\partial \xi_i}{\partial x_j} = \underbrace{\frac{\partial u_i}{\partial x_j}(x, \zeta_i - c)}_{\xi_i(x) - (\zeta_i - c)} \frac{\beta\varepsilon^2}{\xi_i(x) - (\zeta_i - c)},$$

where the terms with underbraces are available from CHARMM.

D. Sampling

We would like to estimate the statistical error of g_j . Ideally, we want the statistical error smaller than some given tolerance with 95% confidence. The sampling error of g_j comes from that of D_j and $(\nabla F)_j$. However, the statistical error of D_j is much smaller than that of $(\nabla F)_j$. Thus, we neglect the statistical error of D_j in estimating the error of g_j . An error bar can be obtained using block averaging in Ref.⁷ (Appendix D.3). In general, 32 blocks is a reasonable choice. Define the error bar of a vector to be as the maximum of the error

bars for each component of the vector. In our example of alanine dipeptide, the statistical error of D_j is neglected. Then, the statistical error of g_j comes from the sample average of $\hat{g}_j^n := \beta D_j (\nabla F)_j^n$, $n = 1, 2, \dots, N$, where N is the sample size. The statistical error is defined by

$$\frac{\max_{0 \leq j \leq J} \text{error bar of } \hat{g}_j}{\max_{0 \leq j \leq J} \|D_j (\nabla F)_j\|_\infty}.$$

At each iteration, the configuration x from the previous iteration could be used to start the equilibration of the molecular dynamics. Thus, it is necessary that values of x be stored such that $\xi(x) = Z_j$, $j = 0, 1, \dots, J$. It is reasonable to expect less equilibration time is needed in later iterations as the path converges.

V. NUMERICAL TESTS

A. An artificial problem

As an example to illustrate our method, consider a problem finding the MFTP and MFEP for the potential energy function

$$U(x, y) = -4 \exp(-4x^2 - (y - 2.75)^2) - 5 \exp(-(x - 1)^2 - (y - 0.15)^2) \\ - 5 \exp(-(x + 1)^2 - y^2) + 8 \exp(-x^2 - (y + 0.5)^2).$$

where units are kcal/mol and M has identical diagonal entries. Unless specifically mentioned, the inverse temperature $\beta^{-1} = 0.59595$, corresponding to 300 K. In particular, we take collective variables $\zeta = \xi(x) = x$. In this case, the MFEP becomes a minimum free energy path (MEP).

In Fig. 3, we show an MEP connecting two local minima through the third local minimum. The MEP has a cusp at the intermediate minimum. The MEPs are computed using the simplified string method with piecewise linear interpolation and equal arc length normalization. The time step $\tau^2 = 0.0025$. The iteration is stopped if $d < 0.005$, some tolerance value, where $d = \max_{0 \leq j \leq J} \tau^{-2} |Z_j^{\text{new}} - Z_j|$. From the figure, we can see that the cusp is missing if the number of images ($J + 1 = 10$) is too small. Also, the MEP does not go through the intermediate local minimum as it should go even with many images ($J + 1 = 80$).

The MFTP avoids the cusp problem; thus, it is a more efficient method than the MFEP in this case. Also, the MFTP generates a different path, same as the MFEP at zero temperature

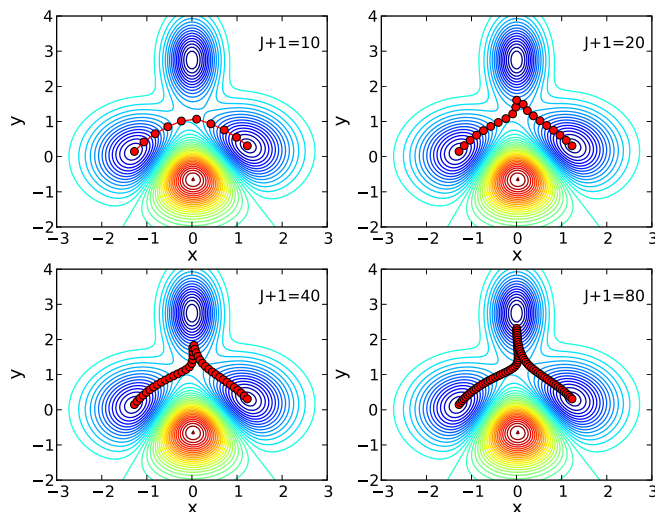


FIG. 3: Minimum energy path obtained using simplified string method. The initial path is the straight line between $(-1, 0)$ and $(1, 0)$. The path is discretized into $J + 1$ images, and we use piecewise linear interpolation and equal arc length normalization. Four figures are generated using $J + 1 = 10, 20, 40, 80$ images, respectively.

but different at others. At infinitely high temperature, one can imagine that all paths are likely with shorter paths more likely; and the center of these paths is the straight line. In fact, our BD model Eq. (3) is purely diffusive at $T = \infty$. The MFTP can be obtained using a relatively small set of images, for example, the MFTP calculated by only 10 images ($J = 9$) is almost indistinguishable as the one calculated using 80 images ($J = 79$). However, the time step for the MFTP is slightly smaller than that for the MFEP when the number of images is large. Fig. 4 shows MFTPs for different temperature. It is clear that the MFTP is close to the MEP at low temperature (3 K), and is close to a straight line at high temperature (3000 K).

B. Phi, psi for alanine dipeptide in vacuum

For comparison with the MFEP, we study alanine dipeptide at 300 K in vacuum¹⁵. We compare the minimum free energy path and the maximum flux transition path with two dihedral angles phi and psi as collective variables. All simulations were performed using

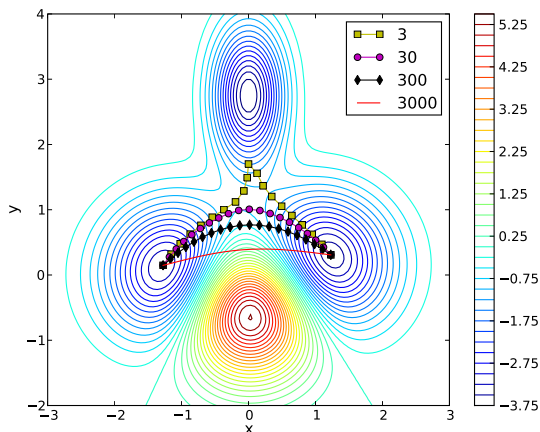


FIG. 4: Maximum flux transition path obtained using simplified string method. Here we used the same initial path, same interpolation and normalization, same stopping criterion for convergence as described in Fig. 3. The MFTPs are generated using 20 images at 3 K, 30 K, 300 K, 3000 K, respectively.

the CHARMM simulation program and the full-atom representation of the molecule in the CHARMM force field¹⁴. Langevin dynamics with friction coefficient 10.0 ps^{-1} and time step 1.0 fs was used. For the calculation of ∇F and D , harmonic potentials as in Eq. (9) were added involving the dihedral angles phi and psi with force constant $1000 \text{ kcal}/(\text{mol rad}^2)$ (corresponding to $\varepsilon = 0.0244 \text{ rad}$).

The initial path in collective variable space is simply a straight line between two points in phi-psi space. The path is discretized into $J + 1$ images. The configuration of alanine dipeptide at each image along the initial path is built using the IC module in CHARMM with dihedral angles fixed at the interpolated values. Then follows 1000 steps of minimization and 50,000 steps of heating before iteration starts. Each iteration of the path involves 50,000 steps of equilibration and 500,000 steps of sampling. The configuration in the last step of sampling is used as the initial configuration for the equilibration in the next step.

We begin by comparing the MFTP and MFEP from $C_{7\text{eq}}$ to $C_{7\text{ax}}$. The MFTP and MFEP are calculated using simplified string method with linear interpolation between images and equal arc length normalization. In Fig. 5, the initial path is the straight line between $(-83.2^\circ, 74.5^\circ)$ and $(70^\circ, -70^\circ)$, which were determined as $C_{7\text{eq}}$ and $C_{7\text{ax}}$ in Ref.¹⁵. The path is discretized into 20 images. The time step $\tau^2 = 0.04$ in CHARMM time units

squared, or $\tau^2 = (9.78 \text{ fs})^2$. The statistical error estimated by block averaging using 32 blocks is $\pm 1.13\%$. The iteration is stopped if $d < 0.02$. (The tolerance value should be chosen properly since the statistical error will eventually dominate the other errors so that d fluctuates about a positive number.) It takes 126 and 128 iterations to converge for the MFTP and MFEP, respectively. The computational cost for two methods is comparable.

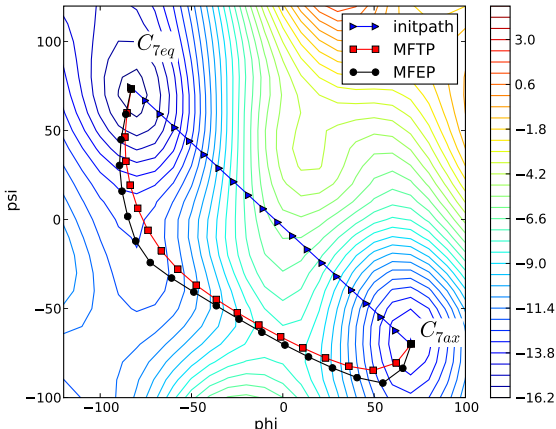


FIG. 5: Maximum flux transition path and minimum free energy path from C_{7eq} to C_{7ax} for alanine dipeptide in vacuum at 300 K. Triangles are images of the initial path; rectangles are the images of the maximum flux transition path; and circles are the images of the minimum free energy path.

Next we compare the MFTP and MFEP from C_{7eq} to C'_{7eq} . In particular, we calculate the transition path $C_{7eq}-C_{7ax}-C'_{7eq}$, in which C_{7ax} serves as an intermediate metastable state. The initial path is taken to be the straight line between $(-80^\circ, 80^\circ)$ and $(190^\circ, -190^\circ)$. Fig. 6 shows the MFEP generated using 40 images. The time step $\tau^2 = (9.78 \text{ fs})^2$. The iteration is stopped if $d < 0.02$. It takes 155 iterations to converge for the MFEP using 40 images. Clearly the MFEP has a cusp at C_{7ax} . Fig. 7 shows the MFTP and MFEP obtained by the simplified string method using 20 images along the path. The time step and the stopping criterion are the same as in Fig. 6. It takes 139 and 140 iterations to converge for MFTP and MFEP, respectively. The cusp of the MFEP is less evident in this case. It requires either many images or adaptive strategies to calculate MFEP; thus, MFTP is more efficient than MFEP.

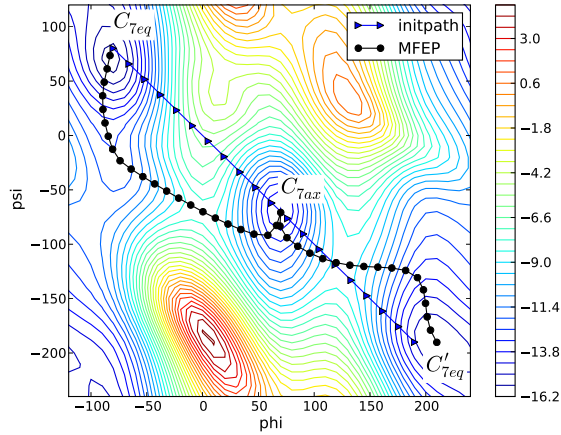


FIG. 6: Minimum free energy path for alanine dipeptide from C_{7eq} to C'_{7eq} passing by C_{7ax} in vacuum at 300 K. The figure is generated using 40 images. Triangles are the images for the initial path; rectangles are the images of the maximum flux transition path; and circles are the images of the minimum free energy path.

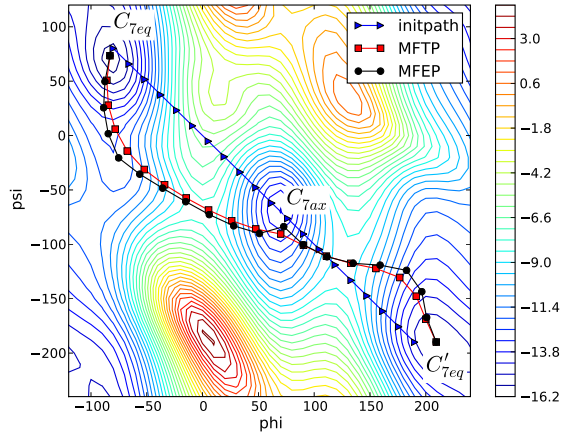


FIG. 7: Maximum flux transition path and minimum free energy path for alanine dipeptide from C_{7eq} to C'_{7eq} passing by C_{7ax} in vacuum at 300 K. The figures are generated using 20 images. Triangles are the images for the initial path; rectangles are the images of the maximum flux transition path; and circles are the images of the minimum free energy path.

VI. CONCLUSION

The method presented here is consistent with the transition path theory. The maximum flux transition path provides a rational finite-temperature correction to the minimum free energy path. The minimum free energy path has cusps at some intermediate metastable states, which makes it unsuitable for defining an isocommittor, unsuitable for defining a reaction coordinate, and harder to compute.

Acknowledgments

This material is based upon work supported by grant R01GM083605 from the National Institute of General Medical Sciences, award A5286056128 from the University of Minnesota, and by a 2007 Purdue Research Foundation Special Incentive Research Grant. We would like to thank Carol Post for the collaboration that nurtured this work. Also, thanks to He Huang for an initial implementation of the string method and an early demonstration of cusps for alanine dipeptide, and to Voichita Dadarlat for Figure 2. Additionally, thanks to Eric Vanden-Eijnden for helpful information about transition path methods and theory. Finally, thanks to the Center for Biological Physics at Arizona State University and the Institute for Mathematics and Its Applications at the University of Minnesota for providing environments that facilitated this work.

APPENDIX A: DERIVATION OF THE MAXIMUM FLUX CONDITION

The assumption that isocommittors are planar implies that the label $s = \sigma(\zeta)$ of the isocommittor passing through ζ satisfies

$$n(\sigma(\zeta)) \cdot (\zeta - Z(\sigma(\zeta))) = 0.$$

Differentiating w.r.t. ζ , we get

$$(n_s(\sigma) \cdot (\zeta - Z(\sigma)) - n(\sigma) \cdot Z_s(\sigma)) \nabla \sigma + n(\sigma) = 0$$

whence

$$\nabla \sigma = (n(\sigma) \cdot Z_s(\sigma))^{-1} e^{-\chi(\sigma, \zeta)} n(\sigma) \quad \text{where } \chi(s, \zeta) = \log \left(1 - \frac{n_s(s) \cdot (\zeta - Z(s))}{n(s) \cdot Z_s(s)} \right).$$

We have

$$\nabla q \approx \nabla \bar{q}(\sigma) = \bar{q}_s(\sigma) \nabla \sigma = \bar{q}_s(\sigma) (n(\sigma) \cdot Z_s(\sigma))^{-1} e^{-\chi(\sigma, \zeta)} n(\sigma),$$

and, consequently,

$$j(\zeta) \approx \psi(\sigma(\zeta), \zeta)$$

where

$$\psi(s, \zeta) = \text{const}_\xi e^{-\beta F(\zeta) - \chi(s, \zeta)} \bar{q}_s(s) (n(s) \cdot Z_s(s))^{-1} n(s)^\top \bar{D}(s) n(s) / |n(s)|.$$

We have

$$\frac{\psi_\zeta}{\psi} = -\beta \nabla F + \frac{n_s}{n \cdot Z_s - n_s \cdot (\zeta - Z)},$$

and

$$\left. \frac{\psi_\zeta}{\psi} \right|_{\zeta=Z} = -\beta \nabla F + \frac{n_s}{n^\top Z_s}.$$

Note that

$$\frac{\nabla j}{j} \approx \frac{\psi(\sigma(\zeta), \zeta)_\zeta}{\psi(\sigma(\zeta), \zeta)} = \frac{\psi_\zeta(\sigma(\zeta), \zeta)}{\psi(\sigma(\zeta), \zeta)} + \frac{\psi_s(\sigma(\zeta), \zeta)}{\psi(\sigma(\zeta), \zeta)} \nabla \sigma(\zeta),$$

and

$$\left. \frac{\nabla j}{j} \right|_{\zeta=Z} \approx -\beta \nabla F + \frac{n_s}{n^\top Z_s} + \frac{\psi_s(s, Z) e^{-\chi(s, \zeta)}}{\psi(s, Z) n(s)^\top Z_s(s)} n.$$

Hence, the condition is that

$$-\beta \nabla F + \frac{n_s}{n^\top Z_s} \parallel n.$$

* Electronic address: rzhao@cs.purdue.edu

† Electronic address: skeel@cs.purdue.edu

‡ Electronic address: shen12@purdue.edu

¹ P. G. Bolhuis, D. Chandler, C. Dellago, and P. L. Geissler. Transition path sampling: Throwing ropes over rough mountain passes, in the dark. *Annu. Rev. Phys. Chem.*, 53:291–318, 2002.

² P. G. Bolhuis, C. Dellago, and D. Chandler. Reaction coordinates of biomolecular isomerization. *PNAS*, 97:5877–5882, 2000.

³ B. R. R. Brooks, C. L. L. Brooks, A. D. D. Mackerell, L. Nilsson, R. J. J. Petrella, B. Roux, Y. Won, G. Archontis, C. Bartels, S. Boresch, A. Caffisch, L. Caves, Q. Cui, A. R. R. Dinner, M. Feig, S. Fischer, J. Gao, M. Hodoscek, W. Im, K. Kuczera, T. Lazaridis, J. Ma, V. Ovchinnikov, E. Paci, R. W. W. Pastor, C. B. B. Post, J. Z. Z. Pu, M. Schaefer, B. Tidor, R. M. M.

- Venable, H. L. L. Woodcock, X. Wu, W. Yang, D. M. M. York, and M. Karplus. Charmm: The biomolecular simulation program. *J. Comp. Chem.*, 30:1545–1614, 2009.
- ⁴ W. E, W. Ren, and E. Vanden-Eijnden. Simplified and improved string method for computing the minimum energy paths in barrier-crossing events. *J. Chem. Phys.*, 126:164103, 2007.
- ⁵ W. E and E. Vanden-Eijnden. Metastability, conformation dynamics, and transition pathways in complex systems. In S. Attinger and P. Koumoutsakos, editors, *Multiscale Modelling And Simulation*, pages 35–68. Springer Verlag, 2004.
- ⁶ W. E and E. Vanden-Eijnden. Towards a theory of transition paths. *J. Stat. Phys.*, 123:503–523, 2006.
- ⁷ D. Frenkel and B. Smit. *Understanding Molecular Simulation From Algorithms to Applications*, 2nd ed. Academic Press, 2002.
- ⁸ W. Gan, S. Yang, and B. Roux. Atomistic view of the conformational activation of Src kinase using the string method with swarms of trajectories. *Biophys. J.*, 94:L01–L03, 2009.
- ⁹ H. Huang. Personal communication, 2008.
- ¹⁰ H. Huang, E. Ozkirimli, and C. B. Post. Comparison of three perturbation molecular dynamics methods for modeling conformational transitions. *J. Chem. Theory Comput.*, 5:1304–1314, 2009.
- ¹¹ S. Huo and J. E. Straub. The MaxFlux algorithm for calculating variationally optimized reaction paths for conformational transitions in many body system at finite temperature. *J. Chem. Phys.*, 107:5000–5006, 1997.
- ¹² H. Jónsson, G. Mills, and K. W. Jacobsen. Nudged elastic band method for finding minimum energy paths of transitions. In B. J. Berne, G. Ciccotti, and D. F. Coker, editors, *Classical and Quantum Dynamics in Condensed Phase Simulations*, page 385. World Scientific, Singapore, 1998.
- ¹³ M. Lei, M. I. Zavodszky, L. A. Kuhn, and M. F. Thorpe. Sampling protein conformations and pathways. *J. Comput. Chem.*, 25:1133–1148, 2004.
- ¹⁴ J. A. D. MacKerell, M. Feig, and I. C. Brooks. Extending the treatment of backbone energetics in protein force fields: limitations of gas-phase quantum mechanics in reproducing protein conformational distributions in molecular dynamics simulations. *J. Comput. Chem.*, 25:1400–1415, 2004.
- ¹⁵ L. Maragliano, A. Fischer, E. Vanden-Eijnden, and G. Ciccotti. String method in collective

- variables: Minimum free energy paths and isocommittor surfaces. *J. Chem. Phys.*, 125:024106, 2006.
- ¹⁶ P. Metzner, C. Schütte, and E. Vanden-Eijnden. Illustration of transition path theory on a collection of simple examples. *J. Chem. Phys.*, 125:084110, 2006.
- ¹⁷ L. Onsager. Initial recombination of ions. *Phys. Rev.*, 54:554–557, 1938.
- ¹⁸ E. Ozkirimli and C. B. Post. Src kinase activation: A switched electrostatic network. *Protein Sci.*, 15:1051–1062, 2006.
- ¹⁹ A. C. Pan, D. Sezer, and B. Roux. Finding transition pathways using the string method with swarms of trajectories. *J. Phys. Chem. B*, 112:3432–3440, 2008.
- ²⁰ W. Ren, E. Vanden-Eijnden, P. Maragakis, and W. E. Transition pathways in complex systems: Application of the finite-temperature string method to the alanine dipeptide. *J. Chem. Phys.*, 123:134109, 2005.
- ²¹ J. Schlitter, M. Engels, and P. Krüger. Targeted molecular dynamics: A new approach for searching pathways of conformational transitions. *J. Mol. Graph.*, 12:84–89, 1994.
- ²² N. Singhal and V. S. Pande. Error analysis and efficient sampling in Markovian state models for molecular dynamics. *J. Chem. Phys.*, 123:4909, 2005.
- ²³ E. Vanden-Eijnden. Transition path theory. In K. Binder, G. Ciccotti, and M. Ferrario, editors, *Computer Simulations in Condensed Matter: From Materials to Chemical Biology, Volume 2*, Lecture Notes in Physics, pages 453–493. Springer, Berlin, 2006.
- ²⁴ E. Vanden-Eijnden, M. Venturoli, G. Ciccotti, and R. Elber. On the assumptions underlying milestoning. *J. Chem. Phys.*, 129:174102, 2008.
- ²⁵ S. Yang, N. K. Banavalib, and B. Roux. Mapping the conformational transition in Src activation by cumulating the information from multiple molecular dynamics trajectories. *PNAS*, 106:3776–3781, 2009.
- ²⁶ R. Zhao. Mftp code, June 2009. URL <http://bionum.cs.purdue.edu/mftp>.